AIAA AVIATION Forum
22-26 June 2015, Dallas, TX
21st AIAA/CEAS Aeroacoustics Conference

10.2514/6.2015-2985

Analytical Prediction of the Pylon-Wake Effect on the Tonal Noise Radiated by the Front Rotor of CROR Propulsion Systems

N. Jaouani*
Sogeti High Tech, Blagnac, 31703, France

M. Roger†
Ecole Centrale de Lyon, Ecully, 69143, France

T. Nodé-Langlois‡
Airbus Operations S.A.S, Toulouse, 31060, France

G. Serre§
Sogeti High Tech, Blagnac, 31703, France

The present paper aims at predicting the tonal noise radiated from the first propeller of *Counter-Rotating Open Rotors* (CROR) in a pusher configuration, considering both the pylon-wake and the uniform flow effects. The computations are carried out in the frequency domain according to Ffowcs Williams and Hawkings' analogy. In order to point out the role of the steady-state source mechanisms in the blade reference frame, three noise sources are identified in the process. First the unsteady loading is computed using a similar procedure to the one used for the rotor-rotor wake interaction noise prediction. The velocity deficit in the wake is locally expanded in two-dimensional Fourier gusts in a reference frame attached to the front rotor. The unsteady lift induced by each gust on a blade segment is calculated using a linearized analytical response function that accounts for a realistic geometry. The steady loading constitutes the second source contribution and is computed using a software based on the lifting-line theory. To ensure an accurate interference of sources, the resulting compact loads are distributed on the same blade geometry that the one used for the unsteady loading computation. Finally the thickness noise due to the blade volume displacement is included in the analysis using Isom's approach. From the linear acoustic assumptions all these sources are modelled as equivalent rotating dipoles and then summed to calculate the far-field noise. The whole methodology is then assessed against wind-tunnel test data. A parametric study considering several pylon positionings and pylon-wake configurations with blowing is finally performed in order to emphasise the relative contribution of the three noise sources.

Nomenclature

Acronyms

BPF	Blade Passing Frequency
CROR	Counter-Rotating Open Rotors
MCL	Mean-Camber Line
MCS	Mean-Camber Surface
PCA	Pitch Change Axis

Symbols

ρ_0	Mean flow density
ω	Angular frequency

*PhD Candidate, Acoustic department, Avenue Escadrille Normandie Niemen, nassim.jaouani@sogeti.com.
†Professor, Laboratoire de Mécanique des Fluides et d'Acoustique, 36 avenue Guy de Collongue, AIAA Member.
‡Research engineer, Numerical Acoustics Group, 316 Route de Bayonne.
§Research engineer, Acoustic department, Avenue Escadrille Normandie Niemen.

ω_m	Harmonic of the blade angular frequency, $\omega_m = mB\Omega$
Ω	Dipole angular velocity = Rotor angular velocity
B	Front-rotor blade number
c_0	Sound speed
C_p	Pressure coefficient
D_c	Doppler factor, $D_c = 1 - M_0 \cos\theta_e$
$\mathbf{F}$	Acoustic dipole force
$\mathbf{F_0}$	Steady Fourier coefficient associated to $\mathbf{F}$, $\mathbf{F_0} = \mathbf{F_s} + \mathbf{F_t}$
$\mathbf{F_s}$	Fourier coefficient associated to the steady loading
$\mathbf{F_t}$	Fourier coefficient associated to the dipole force responsible for thickness noise
J_n	m-th order Bessel function of the first kind
k	Gust circumferential index = Loading harmonic index
m	Acoustic mode index associated to the rotor radiation
M_0	Mean flow Mach number, $M_0 = U_0/c_0$
n	Acoustic mode index associated to the dipole radiation
$\mathbf{n}$	Blade local unit normal vector
$\tilde{p}$	Complex acoustic pressure
(R, θ, ϕ)	Observer spherical physical coordinates
(R_e, θ_e, ϕ)	Observer spherical emission coordinates
(R_0, ϕ_0, x_0)	Source cylindrical coordinates
t	Time value
$\mathbf{x}$	Observer position

I. Introduction

The CROR propulsion system is a possible alternative to turbofan engines for middle-range aircrafts. Reducing significantly the fuel consumption and the dioxide carbon emissions,[1] it could represent a solution to reach the ACARE goals and is investigated intensively by the aircraft and engine manufacturers and the research community. Also called CRP for *Counter Rotating Propellers* this propulsion system is composed of two propellers rotating in opposite directions around the same engine axis. The swirl of the flow induced by the first propeller is recovered by the second propeller providing a gain of propulsive efficiency. If this technology ensures larger by-pass ratios than turbofan engines improving again their propulsive efficiency, it may lead to increased radiated noise levels since the absence of duct excludes all possible acoustic liners. Complying with the current thresholds of community noise certification and cabin comfort is a major challenge of CROR engines and the noise radiation has to be reduced directly at source by acting on the emission mechanisms.

The CROR engine is characterized by many sources generating two types of tonal noise, rotor-alone tones at the harmonics of each Blade Passing Frequency (BPF) and combination tones between the two rotors at linear combinations of both BPF. In the case of an isolated CROR at low speed, it has been shown that the *interaction noise* generated by the impingement of wakes from the front propeller on the rear propeller is the dominant noise component.[2] A lot of work has been done to describe this mechanism and many strategies exist to evaluate the resulting radiated noise both analytically[3] and numerically.[4,5,6] Numerically, an attractive strategy is the CFD chorochronic (phase-lagged) approach that allows to consider only a single blade passage during the unsteady simulations and therefore offers significant CPU time savings[7] compared to full-annulus direct simulations. However the chorochronic technique based on the natural space (choro) and time (chronic) periodicity of the flow in a turbomachinery is only available for isolated configurations assuming a uniform and purely axial mean speed associated with forward flight. The integration of a CROR on the aircraft leads to non-homogeneous inflows induced by the so-called aerodynamic installation effects. For the pusher configuration (see figure 1), where the CROR is mounted on the rear fuselage, this is represented mainly by the pylon wake which impinges both propellers whereas for the puller configuration, where the CROR is in front of the wing, the distortion arises from the wing upwash. As a non-axisymmetric flow feature, this source mechanism cannot be dealt with the chorochronic approach. Considering the high computational cost necessary to simulate the unsteady flow over the complete geometry, the use of analytical approaches remains a good candidate in a design optimization process.

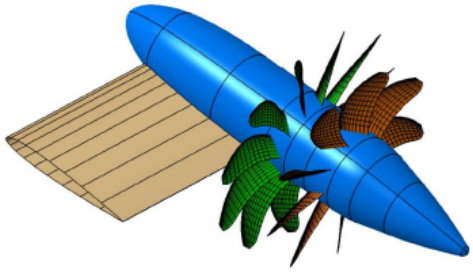

Figure 1: Counter-Rotating Open Rotor system in pusher configuration.

In this study, we address the pusher configuration and only the pylon-wake effect on the front-rotor BPF since it is believed to be more pronounced than the pylon-wake effect on the rear-rotor BPF and on the rotor-rotor interaction tones.[8,9,10] As for the interaction noise, the methodology follows three steps: the description of the pylon wake impinging on the front propeller, the computation of the induced blade loading and the radiated noise computation. In order to identify all inputs required by the analytical formulation, it is chosen to describe first the noise produced by a rotating blade element. According to Ffowcs Williams and Hawkings' analogy,[11] the noise results from the contribution of acoustic monopole, dipole and quadrupole sources. However it can be shown that equivalent dipoles can replace the monopole term.[12,13] Considering the current fully subsonic flows and thin-blade design, the quadrupole sources accounting for viscous and propagation effects in the flow surrounding the blades can be neglected.[14] The noise radiation of the front propeller impinged by the pylon wake can then be reduced to dipole source evaluation. This is described in section II. The blade-loading computation strategy is described in section III. Its unsteady component should be responsible for the major part of the noise radiation. However the steady loading induced by the mean flow is included in the analysis since it contributes to the main radiation lobes. The 3D blade geometry is considered and both steady and unsteady loads are projected on the mean-camber surface. The resulting noise levels are then compared to wind-tunnel test data in section IV to point out the interference effects between the noise contributions. The polar microphone line being fixed in the measurements, three different azimuthal locations of the pylon are assessed in section V in order to investigate the pylon positioning relative to the observer. Finally the wake-blowing technology is assessed by predictions and again compared with measurements in section VI. In all the methodology the pylon wake, the accurate description of which is essential to the noise evaluation, is supposed to be known and extracted from CFD simulations.

II. Analytical Model of Pylon-Induced Front-Rotor Tones

Various formulations have been proposed to describe the noise radiated by isolated CROR. Most of them are dedicated to the interaction noise prediction since it is believed to be the main source mechanism.[15] In addition a specific effort has been made to consider a well suited geometry both for the loading computation and for the source location.[3] For an installed CROR these formulations can easily be adapted to evaluate the pylon-wake effect on the front-propeller BPF tones. Indeed the pylon/front-rotor can be seen as a doublet generating an *interaction noise* equivalent to the noise produced in rotor-rotor interaction. In this case the pylon is assimilated to a propeller composed of one blade with zero angular velocity. However this procedure has the drawback of predicting only the loading noise contribution. Another classical way consists in considering the pylon wake as a non-homogeneous inflow of the front propeller. In this case, the Hanson and Parzych formulation[16] can be used, resulting in separate formulas for the loading and thickness noise contributions. In 1975, Isom showed[12] that in far field the thickness noise contribution of a hovering helicopter rotor blade is equal to the noise produced by a dipole source induced by a uniform pressure distribution over the entire blade surface. Extended by Farassat for any body in arbitrary motion,[13] this approach does not require the usual evaluation of the normal velocity, very sensitive to the mesh size. Therefore a new procedure is developed in which each blade element is associated to two dipole sources: the one associated to the blade loading and the one accounting for the blade volume displacement. Both contributions are then summed linearly.

The objective of this section is to give a general formula for the rotating dipole in forward flight and to identify the dipole force in each noise contribution. A frequency-domain formulation is selected assuming geometrical and acoustical far field. As in Hanson and Parzych formulation,[16] a cylindrical coordinate system is used to describe the dipole force since it highlights the components that have a significant noise contribution. For simplicity the forward flight is supposed purely axial. The corresponding formula can be found in Carazo *et al.*[3] as an intermediate result and gives the resulting pressure for an observer located at $\mathbf{x}$ as:

$$\tilde{p}(\mathbf{x},\omega) = \frac{\mathrm{i}\omega}{4\pi R_e D_c c_0} \mathrm{e}^{\mathrm{i}\omega\left(\frac{R_e}{c_0}+\frac{\cos\theta_e}{D_c c_0}x_0\right)} \sum_{n=-\infty}^{+\infty} \mathrm{e}^{\mathrm{i}n\left[\phi-\frac{\pi}{2}-\phi_0\right]} \left[\left\{\frac{\cos\theta_e}{D_c}\tilde{F}_A(\omega-n\Omega) + \frac{nc_0}{\omega R_0}\tilde{F}_T(\omega-n\Omega)\right\} \mathrm{J}_n\left(\frac{\omega R_0 \sin\theta_e}{D_c c_0}\right) + \mathrm{i}\frac{\sin\theta_e}{D_c}\tilde{F}_R(\omega-n\Omega)\mathrm{J}'_n\left(\frac{\omega R_0 \sin\theta_e}{D_c c_0}\right)\right], \quad (1)$$

where (R,θ,ϕ) are the observer spherical coordinates in a frame centered at the constant axial position of the dipole. (R_e,θ_e) are the emission coordinates for a flow of Mach number M_0 in the X direction (R_e being the same for all sources). $D_c = 1 - M_0\cos\theta_e$ is the Doppler factor, Ω is the dipole angular velocity and c_0 is the sound speed. (R_0,ϕ_0,x_0) correspond to the cylindrical coordinates of the dipole at $t=0$, and so to the corresponding blade element (see figure 2). The equation involves an infinite sum over the acoustic modes n. In fact, the dipole force harmonics being given by the components in the cylindrical coordinates $\left(\tilde{F}_A,\tilde{F}_T,\tilde{F}_R\right)$, it is found that a signal of frequency ω, perceived by a far-field observer, is produced by a sum of dipole force harmonics of frequencies $\omega - n\Omega$. Finally the noise radiation is determined by the Bessel functions of the first kind J_n and their derivatives J'_n at orders n. In practice the properties of Bessel functions are used to limit the source frequency range and the number of modes to take into account to approximate the infinite sum.

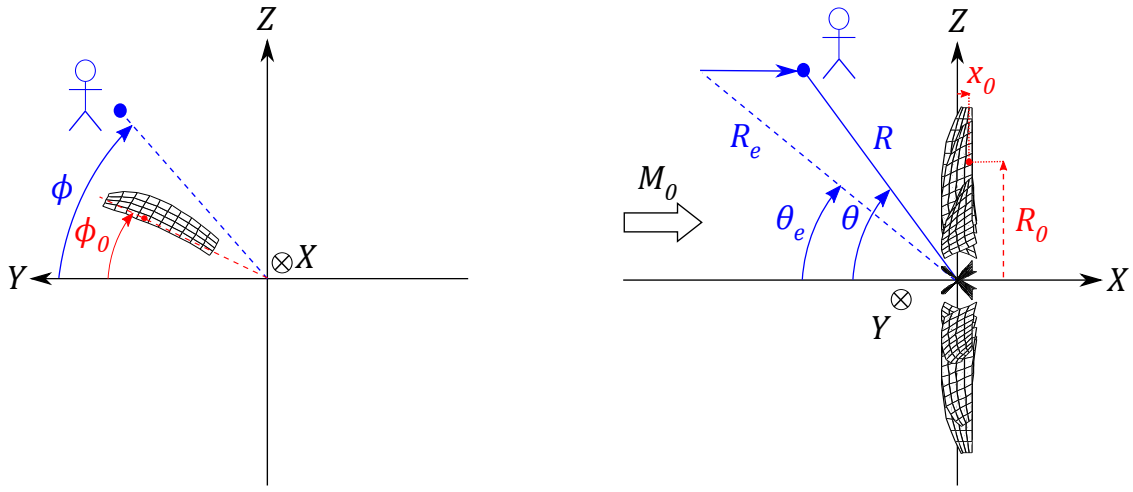

Figure 2: Source (*red*) and observer (*blue*) coordinates considering a front view (*left*) and a side view (*right*) of a propeller scheme.

The next step consists in defining the dipole force and is very similar to what is done for the CROR interaction-noise derivation. The pylon wake is seen periodically in the angular direction by each front-rotor blade. The induced unsteady loadings are therefore periodic in time with fundamental frequency Ω. The steady loading and blade volume displacement being steady mechanisms in the blade reference frame, the dipole force $\mathbf{F}(t)$ can be expanded into the Fourier series

$$\mathbf{F}(t) = \sum_{k=-\infty}^{+\infty} \mathbf{F_k}\mathrm{e}^{-\mathrm{i}k\Omega t} \qquad \text{with} \qquad \mathbf{F_k} = \left(F_k^A, F_k^T, F_k^R\right) = \frac{\Omega}{2\pi}\int_0^{\frac{2\pi}{\Omega}} \mathbf{F}(t).\mathrm{e}^{\mathrm{i}k\Omega t}dt, \quad (2)$$

its Fourier transform for the cylindrical component i being given by

$$\tilde{F}_i(\omega - n\Omega) = \sum_{k=-\infty}^{+\infty} F_k^i \delta\left(\omega - (n+k)\Omega\right) \tag{3}$$

where δ is the Dirac delta function. It must be noted that the steady Fourier coefficient $\mathbf{F_0}$ includes not only the steady loading $\mathbf{F_s}$ but also the dipole force associated with thickness noise $\mathbf{F_t}$.

Next we have to consider not a single dipole but a set of B identical and equally-spaced phased dipoles, B being the blade number of the front rotor. Let us assume that the front rotor is composed of identical and equally-spaced blades, so that the interference effect of multiple dipoles can be modelled by defining a phase lag with respect to a reference dipole and accounting for emission location and time effects. As shown in Hanson's formulation for CROR interaction noise,[15] this finally leads to the formula

$$\begin{aligned}\tilde{p}(\mathbf{x}, \omega_m) = \frac{\mathrm{i}B\omega_m}{4\pi R_e D_c c_0} \sum_{k=-\infty}^{+\infty} \mathrm{e}^{\mathrm{i}\left[\omega_m\left(\frac{R_e}{c_0} + \frac{\cos\theta_e}{D_c c_0}x_0\right) + \xi_{km}\left(\phi - \frac{\pi}{2} - \phi_0\right)\right]} \left[\left\{\frac{\cos\theta_e}{D_c} F_k^A \right.\right. \\ \left.\left. + \frac{\xi_{km} c_0}{\omega_m R_0} F_k^T\right\} \mathrm{J}_{\xi_{km}}\left(\frac{\omega_m R_0 \sin\theta_e}{D_c c_0}\right) + \mathrm{i}\frac{\sin\theta_e}{D_c} F_k^R \mathrm{J}'_{\xi_{km}}\left(\frac{\omega_m R_0 \sin\theta_e}{D_c c_0}\right)\right]\end{aligned} \tag{4}$$

with $\omega_m = mB\Omega$ the blade passing frequency of the front rotor and $\xi_{km} = mB - k$ the order of the Bessel functions.

This formula now requires the blade loading and the dipole force associated with thickness noise $\mathbf{F_t}$ as input. The former is the objective of the next section. The latter can be derived easily using Isom's formulation as the uniform pressure distribution over the entire blade surface

$$\mathbf{F_t} = \rho_0 c_0^2 \mathbf{n}. \tag{5}$$

Here ρ_0 is the density of the mean flow, c_0 the sound speed and $\mathbf{n}$ the local unit normal vector expressed in cylindrical coordinates. Consequently the *dipole thickness noise* is determined only by the current ambient conditions and the blade geometry and kinematics. Validated many times in the literature,[17,18] this formulation does not involve the normal velocity over the blade surface. However it requires to refine properly the blade mesh at the inner and outer radii, and to include the blade-tip source which has a very significant effect on the noise prediction, contrary to the blade hub.[19]

In practice, to evaluate the noise produced by the whole propeller, the equivalent dipole sources associated to each noise contribution should be placed on the same surface to adequately capture the interference effects. Whereas the steady loading can be projected easily on the zero-thickness *Mean-Camber Surface*, required by the unsteady loading computation, the same strategy does not hold for the thickness noise as computed using Isom's formula since it would lead to a zero noise contribution. Therefore the dipole sources associated to thickness noise are maintained on the real blade surface. In addition all elementary sources must be compact with respect to the observer in far field. In terms of geometry, this leads to decompose the whole blade surface and the mean-camber surface in lattices for estimating the thickness and loading noise, respectively.

III. Loadings Induced on the Front Rotor and First Noise Predictions

This section aims at computing the loading induced on the front-rotor blades due to a pylon wake in an otherwise uniform flow, the direction of which is the same as the rotation axis. Whereas the mean flow, being steady in the blade reference frame, involves the so-called *steady loading*, the pylon wake impinges each blade of the front rotor successively inducing the so-called *unsteady loading*. It is worth stressing that the velocity deficit in the wake modifies the mean flow seen by the blade and has an effect on the steady loading. However it is assumed here that this effect is negligible. Consequently in all the following the steady loading will be computed without the pylon in isolated configuration. Two different strategies are chosen to evaluate the mean and fluctuating loads.

A. Unsteady Loading Computation and Associated Noise

The unsteady loading is calculated following the methodology developed by Carazo *et al.*[3] and requires the propeller geometry and the velocity deficit of the pylon wake to be known. The propeller being composed of identical and equally-spaced blades with the same pitch angle, only one reference blade is needed to describe the sources.

A pre-processing of the blade geometry is necessary to define the zero-thickness flat plates required by the unsteady loading model. The 3D blade geometry is first considered via a *Mean-Camber Surface* (MCS) to ensure the zero-thickness requirement. The MCS being split in radial strips, each strip is then interpolated by a trapezoid in order to be at best in accordance with the original geometry (see figure 3). It is worth noting that the trapezoids are dominantly determined by the leading-edge part taking into account the significant unsteady loading at this location.

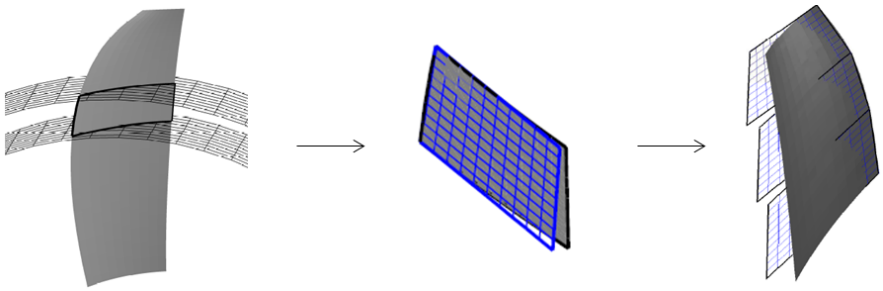

Figure 3: Blade *Mean-Camber-Surface* splitting process (from Carazo *et al.*[3]).

The flow distortion rearward the pylon is described for each strip on a surface in the vicinity of the leading-edge, called *propeller surface* (see figure 4). The pylon wake is obtained using 2D steady RANS numerical simulations on the pylon at scale 1/6. The mesh of the surface from which the velocity field is extracted is refined in order to reach the convergence of the resulting noise levels. Here 121 radial nodes and 721 azimuthal nodes ensure the convergence up to the 5th harmonic of the BPF. It is worth noting that for the present blade geometry the interpolation surface does not need to follow the leading-edge line in first approximation. Even if the results are not included in the present paper, a *propeller disk* located at the axial location of the *Pitch Change Axis* (PCA) was also assessed and allowed to catch the pylon-wake perturbations in a relevant way in terms of resulting noise levels. The flow distortion induces perturbations of the velocity normal to the MCS at leading-edge. The so-called *upwash* is then expanded into sinusoidal oblique gusts with two wavenumbers using a two-dimensional Fourier series in radial and angular directions on each strip.

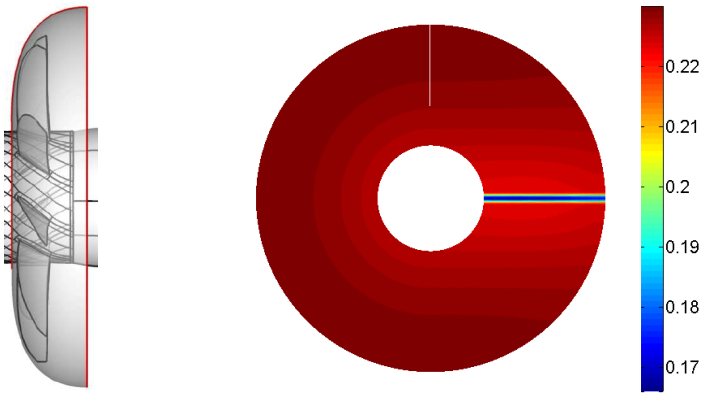

Figure 4: Axial Mach number field (*right*) extracted on the interpolation surface in the vicinity of the front-rotor leading edge (*left*).

The unsteady loads induced on each strip are then computed using the Amiet-Schwarzschild theory,[20] which describes the response of an infinite thin airfoil to an incident "frozen" gust. Here an extended

formulation is considered in which the response function is developed for an isolated trapezoid accounting for a more realistic geometry.[3] The unsteady loading being computed for each strip independently and projected back to the MCS, a phasing of the obtained responses is needed to reproduce the source distribution. This is carried out by computing the time required by the excitation to travel from one strip to another, accounting for the blade leading-edge geometry. Finally a regularization is applied to suppress the discontinuities between adjacent segments. An example of the resulting blade unsteady-loading distribution over the MCS is given in figures 5a and 5b for the loading harmonic $k = 12$. Concentrated at leading edge, the unsteady loading is continuous from one strip to another. Even if its amplitude is assumed to be negligible in comparison to that of the tangential and axial components for the present blade geometry, the radial component of the unsteady loading is included in the analysis since some interference is expected with the volume displacement sources.

(a) Real part (b) Phase (rad)

Figure 5: Blade unsteady-loading distribution induced by the pylon-wake impingement, normalized by the static pressure in free stream (k = 12). A set of 17 trapezoids is used to approximate the blade geometry.

The resulting unsteady-loading noise can be evaluated by summing the noise contributions of all the equivalent dipoles distributed on the MCS given by Eq. 4, ignoring the coefficient of order 0. An example of a calculated spherical directivity, with the propeller geometry of the test campaign, is provided in figure 6 for the first BPF.

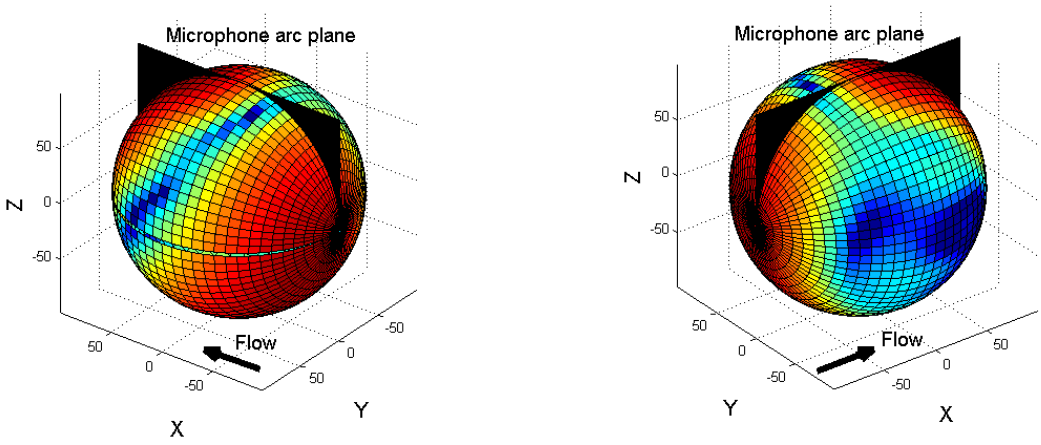

Figure 6: Unsteady-loading noise prediction (m = 1) at R = 99.6m from a pylon-side view (*left*) and a silent-zone-side view (*right*).

The pylon being placed horizontally along the Y > 0 direction (this will be the case for all model predictions in this paper), two patterns can be distinguished, considering the sphere in two halves divided vertically. The pylon-side half exhibits an oblique *silent* plane and the other one an extended *silent* zone. Basically these two patterns can be related to the dipolar nature of the sources and to the blade geometry. Indeed as the blade crosses the pylon wake, the radiation is maximum in a direction perpendicular to the mean blade plane, producing the two significant directivity lobes on the first half sphere. On the contrary, the mean blade plane, inclined according to the blade pitch angle with the horizontal plane during the interaction, leads to a silent plane on the first half sphere which extends to a complete silent zone on the other half. These features are a consequence of the localized character of the flow distortion involved in pylon-wake interaction.

B. Steady Loading Computation and Associated Noise

The steady loading is calculated using the LPC2 software based on the lifting-line theory and developed by ONERA.[21] Computations are performed over a certain number of airfoil sections describing the propeller blades. For each blade, starting from polar inputs (lift and drag coefficients) as functions of the local incidence and Mach number, and a surrounding uniform velocity field, vorticity lattices shed at the trailing edge are defined from the airfoil lift/circulation (Kutta-Joukowski law). The Biot & Savart law is then used to compute the velocity field induced by each lattice. An update of the local incidences and consequently of the sectional aerodynamic coefficients is then applied and an iterative process is launched to reach convergence. This results in a spanwise distribution of 12 compact loads, located at 1/4 chord, expressed only by the axial and tangential components. The radial load component, considering the moderate blade sweep and lean of the present geometry, is assumed negligible in this first estimate, without affecting the interference with other noise sources. However it could have a significant influence for another blade geometry with prominent sweep and lean, especially at blade tip where the vortex flow produces a radial suction force.[22]

An alternative loading distribution is also assessed. Instead of considering the loads as concentrated to very few lattices of the MCS (one lattice is selected for each compact load previously mentioned), they are distributed over the whole MCS. In this way the same geometry is considered for both steady and unsteady loads and the interference between dipoles is better reproduced in the computations. To do that the following procedure is carried out. First each compact load being associated with a cross-section of the blade CAD, the latter is approximated by an equivalent airfoil of the NACA family by tuning the parameters (maximum thickness, maximum camber and its location). The distribution of pressure coefficient Cp over the obtained NACA airfoils are then computed using the XFLR5 numerical software based on XFOIL (see figure 7) providing for each section the angle of attack and the Reynolds number (accounting for induced velocities). The viscous formulation developed in the XFOIL software[23] and suitable for a fast analysis of airfoils at low Reynolds number then leads to neglect 3D effects.

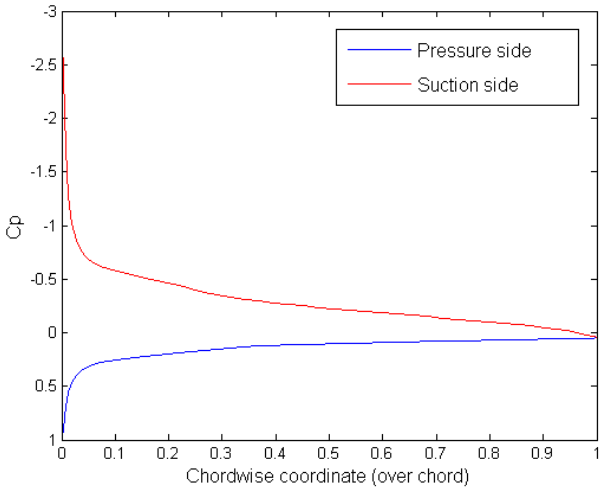

Figure 7: Example of Cp distribution returned by XFLR5 - Section at r/rtip = 0.8.

The Cp distribution over the airfoil allows obtaining the chordwise pressure distribution along the *Mean-Camber Line* (MCL). In acoustic terms, this means taking into account the phase-lags between signals coming from pressure and suction sides of the airfoil. A 3D interpolation is then used to distribute the loading in the spanwise direction of the MCS. Given that a normalization with the total blade thrust and torque is done at each step of the process, it results in a suitable distribution of pressure over the whole MCS. In this case all lattices of the MCS having their own steady loading $\mathbf{F_s}$ radiate noise in the far field, according to Eq. 4.

The noise induced by the two previous steady loading distributions is then assessed against the KIM software selected as a reference. Developed also by ONERA, this tool groups the Ffowcs Williams and Hawkings and Kirchhoff integral methods and calculates the wave propagation over large distances in uniform flows either from a solid or permeable integration surface.[24] As indicated in figure 8, the steady-loading noise prediction is in a good agreement with KIM for both loading distributions. However the projection of the compact loads on the MCS is more relevant at lower θ angles.

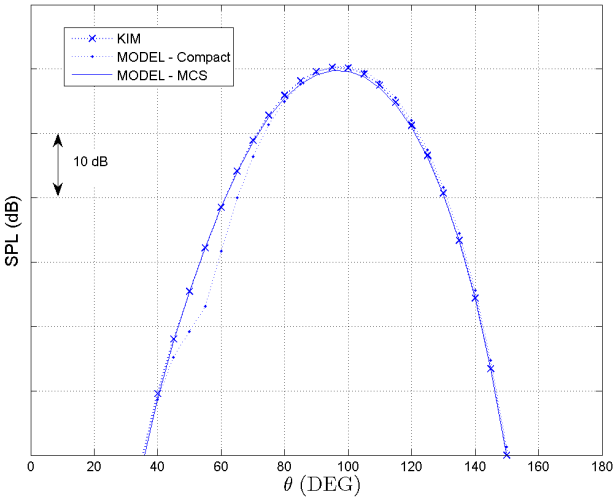

Figure 8: Steady-loading noise prediction (m = 1) at $\boldsymbol{\phi} = 90^\circ$ and comparison with KIM.

IV. Comparison With Test Data

The methodology developed in previous sections is assessed in this part by comparison with wind-tunnel tests. The comparison is based on the DREAM campaign performed in 2008 at DNW. Designed both by Rolls Royce (rig and propellers) and Airbus (pylon), the test rig is made of counter-rotating propellers at scale 1/6 placed in an axial flow of Mach number $M_0 = 0.23$. The pylon has zero sweep and its trailing-edge is located 30% of pylon chord upstream of the propeller PCA. Furthermore the pylon span is oriented to the ground for the present section (see figure 9 (*right*)). The far-field measurements are obtained thanks to wall microphones located outside the wind-tunnel jet. The tones are therefore extracted from the measurements after correction of the jet shear-layer refraction and removal of the background noise. Finally a spherical divergence correction is applied to obtain polar directivities at a reference distance of 16.6m.

In the present study, we are interested in the radiation of the propeller encountering both the mean flow and the pylon wake. First the mean flow effect is evaluated using measurements in isolated configuration. This allows assessing the steady-loading noise plus the thickness noise prediction. In accordance with the measurement microphones, the prediction is carried out at $\phi = 90^\circ$ for both noise contributions. Note that the isolated configuration being axisymmetric, the noise levels are independent of the selected observer azimuthal angle (given the same angle for both steady loading and thickness noise components). However since it will be combined with the unsteady loading noise, this specific azimuthal angle is selected to well return the expected interference. The resulting noise is indicated in figure 10 for the first BPF. Even if the polar directivity is slightly shifted upstream, the analytical prediction can be considered in a good agreement with measurements since only an underprediction of less than 1.5 dB is observed. This slight shift in directivity

Figure 9: DREAM campaign test rig (*left*) and pylon configuration (*right*).

is believed to be related to the thickness noise component evaluation since the single steady-loading noise directivity is well centered and was validated with KIM in previous section. The maximum noise levels are correctly estimated and the total noise prediction associated to the isolated propeller can be considered as reliable in the following. It is worth noting that the second steady-loading distribution over the MCS was selected for the analysis since it was found more reliable than the 12 compact loads, so that the same geometry is used for the definition of both steady and unsteady loads.

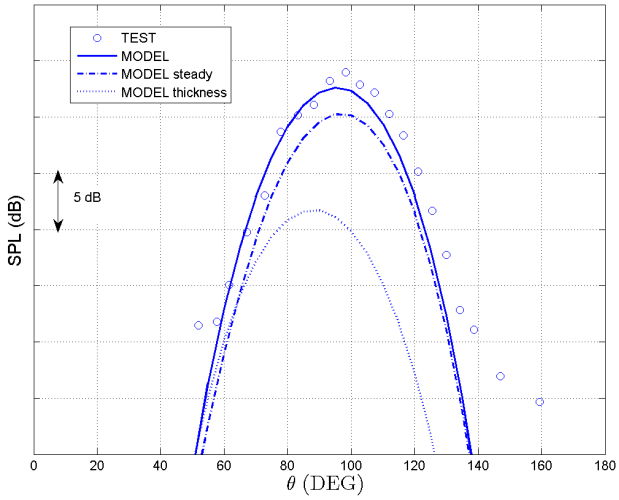

Figure 10: Total noise prediction in isolated configuration (m = 1) at $\phi = 90°$ and comparison with test data.

The unsteady-loading noise computation being performed, the simulation of the microphone arc included in the black plane of figure 6 is considered to be in agreement with measurements. The summation of acoustic complex pressures associated to the three identified source mechanisms then leads to the total noise prediction provided in figure 11. Considering the first noise harmonic in figure 11a, the interference effect between noise sources is clearly pointed out. Given the low noise levels of the thickness component, the significant noise increase around the propeller plane is associated mainly to the interference between the steady and unsteady loading components. In addition this interference leads to shift the silent zone initially observed at 65° upstream of the propeller when computing only the unsteady-loading noise to 60°, which ensures the consistency with test data. Downstream of the propeller, even with more than 20 dB lower than the unsteady-loading noise levels, the steady-loading noise can still have a noticeable effect on the total radiated noise. Nonetheless this conclusion is limited to the first noise harmonic for which the steady-loading noise and the thickness noise reach their maximum values. These noise contributions become completely negligible for higher BPF harmonics for the operating point considered here, as exhibited in figures 11b and

11c. The total noise predictions are described by two features, whatever the noise harmonic, as synthesized in figure 11d. Upstream of the propeller, the silent zone is exagerated by the model and downstream the pylon-wake effect is overpredicted.

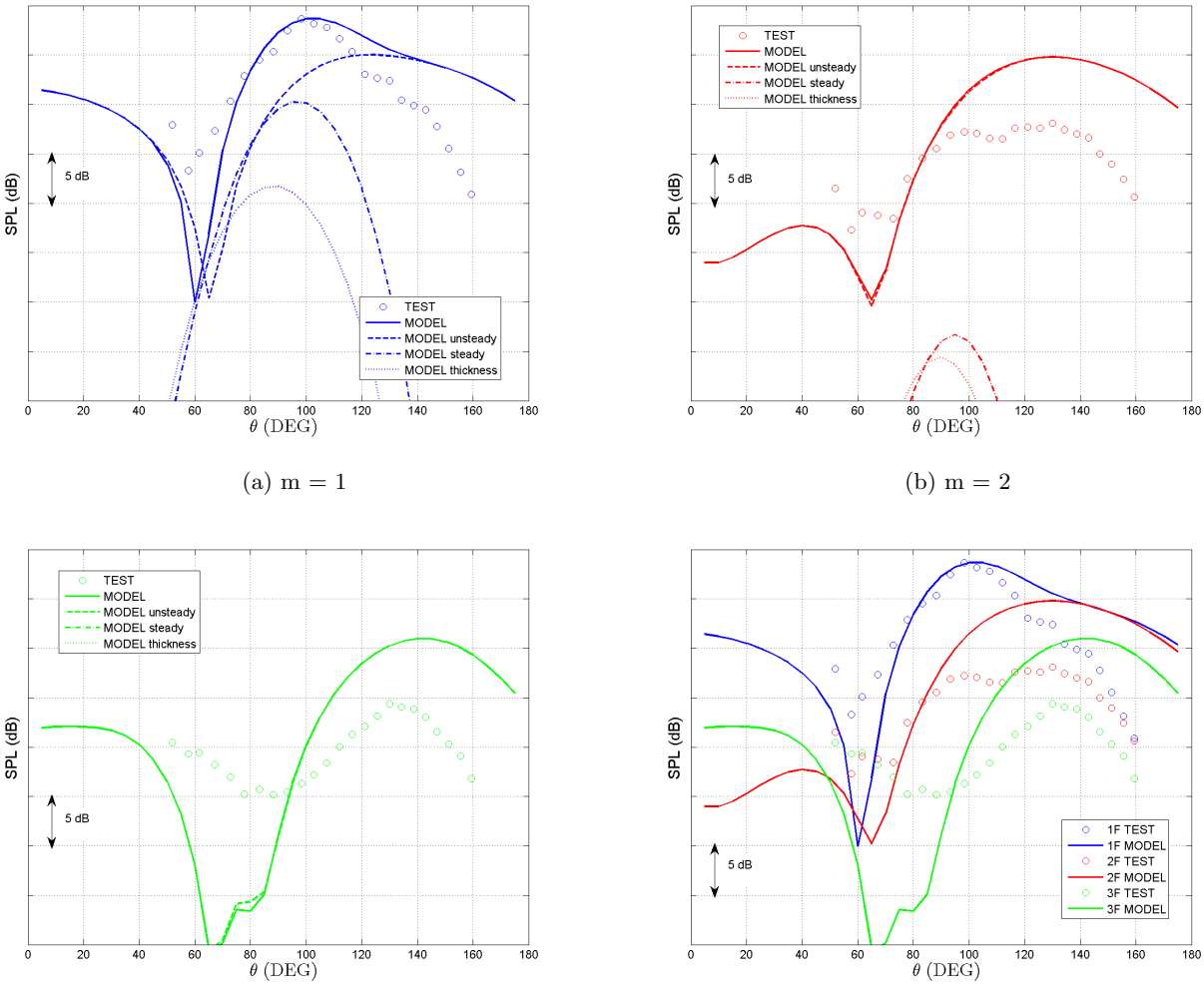

(a) m = 1

(b) m = 2

(c) m = 3

(d) m = 1, 2, 3

Figure 11: Total noise predictions in *PylonBottom* configuration at $\phi = 90°$ and comparison with test data.

Considering the measurement conditions, an attempt can be made to explain the discrepancies. First the current model assumes that the incident flow only involves the pylon wake as a distortion. This assumption should be reviewed given the boundary layer developing on the nacelle in the measurements. In addition the pylon wake extracted from the numerical simulations is subject to uncertainty, which needs to be assessed in terms of resulting noise levels. According to Ricouard *et al.*,[8] a reduction of less than one third of the wake velocity deficit can actually reduce the pylon impact by 2 to 3 dB. Globally the aerodynamic installation effect is therefore qualitatively predicted by the model. Furthermore the model does not take any acoustic installation effect into account. The emitted noise is assumed to propagate directly to the microphones in far field. However in the measurements the pylon diffraction can tend to fulfil partly the silent zone upstream of the propeller. In addition the sound refraction by the propeller streamline tube could induce a decrease of noise levels in the downstream region. These considerations constitute the main guidelines to complete the model in a future work.

V. Sensitivity to Pylon Positioning

In previous section, a single pylon configuration was considered for the model assessment. The polar microphone line being fixed in the measurements, the azimuthal directivity of the pylon-wake interaction with the propeller can however be evaluated considering other pylon positionings. As indicated in figure 12, two other pylon configurations complement the so-called *PylonBottom* configuration of previous section.

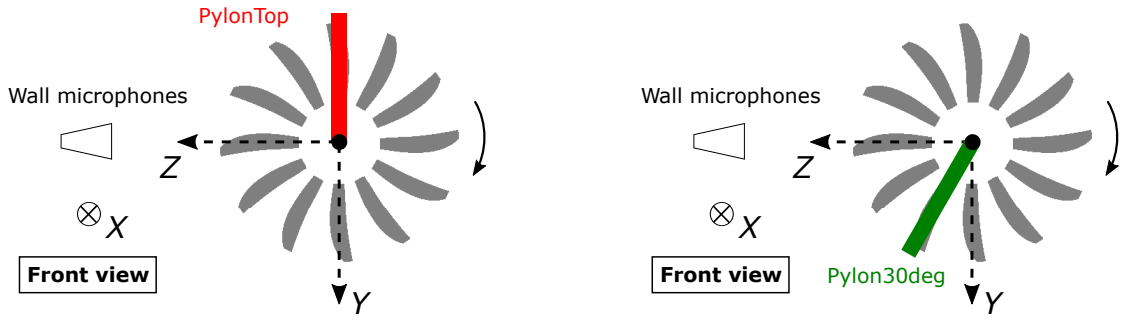

Figure 12: Other pylon configurations assessed in the DREAM campaign: *PylonTop* (*left*) and *Pylon30deg* (*right*).

First the *PylonTop* configuration is opposite to the reference *PylonBottom*, allowing to highlight the sensitivity to the source-to-microphone motion. In terms of noise, referring to figure 13a, this leads to reverse the noise directivity with respect to the propeller axis, with for instance from now on a silent zone downstream of the propeller. In addition the maximum noise level is well reduced in the propeller plane. This is due to the convective amplification since in the *PylonBottom* case, the blade approaches the microphones when crossing the pylon wake whereas it moves away in the *PylonTop* case. As shown in figure 13b, the second noise harmonic exhibits the same trends.

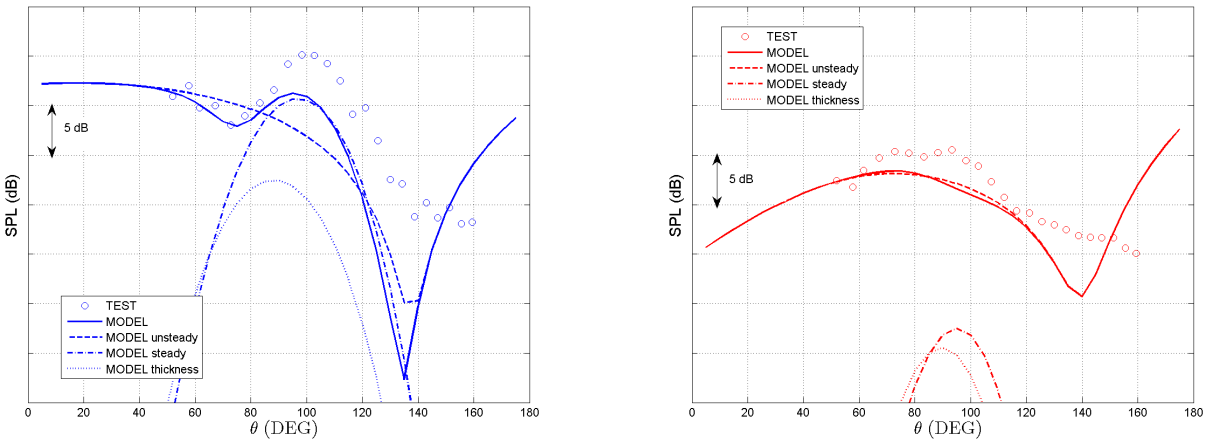

(a) m = 1

(b) m = 2

Figure 13: Total noise predictions in *PylonTop* configuration at $\phi = 270°$ and comparison with test data.

Then, in the so-called *Pylon30deg* positioning, the pylon is located 30° from the *PylonBottom* configuration in the propeller rotation direction (see figures 9 and 12). As pointed out in figures 14a and 14b, the resulting unsteady-loading noise is characterized by a silent zone closer to the propeller plane compared to the *PylonBottom* configuration. Thus the steady source mechanisms become significant and lead to a disrupted total noise directivity, with two silent zones, quite well recovered by the model. The downstream noise is however overpredicted as in previous section. Similarly at the second noise harmonic, the effect of steady source mechanisms becomes negligible.

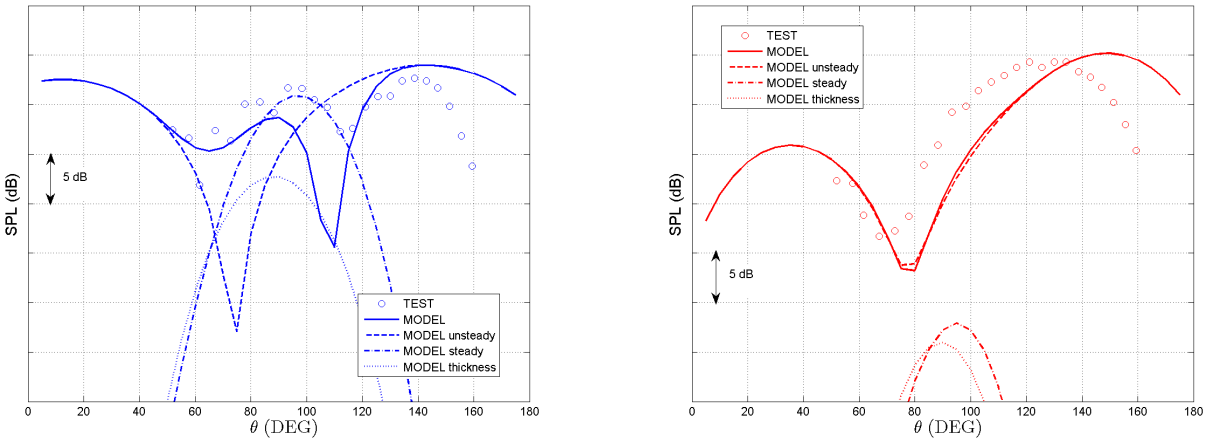

(a) m = 1 (b) m = 2

Figure 14: Total noise predictions in *Pylon30deg* configuration at $\phi = 60°$ and comparison with test data.

VI. Blowing Assessment

This part is dedicated to the previous methodology applied to pylon configurations with blowing. The blowing consists in adding air at the pylon trailing-edge in order to fill the wake velocity deficit. A parametric study has already been done by the authors on a generic pylon wake.[25] Nonetheless the blowing was taken arbitrary and it is not ensured that the resulting generic wake shapes can be obtained in practice. Here the wake shapes with blowing are again extracted from 2D numerical simulations (RANS). The interpolation surface is located in the vicinity of the propeller leading edge in the same way as for figure 4. The resulting noise levels are computed using the complete procedure developed in sections II and III. Assuming again that the steady loading is independent of the pylon wake, the blowing has an effect only on the unsteady-loading noise. The predictions are then compared to measurements coming from the same campaign as in section IV, considering the *PylonBottom* configuration and the arc microphone at $\phi = 90°$ as indicated previously in figure 9. Two flow rates identical to the one of the measurements are selected to make the comparison relevant. The resulting pylon-wake profiles are assessed against the pylon-wake without blowing in figure 15, U and U_0 being the axial velocity components of the pylon wake and the mean flow respectively.

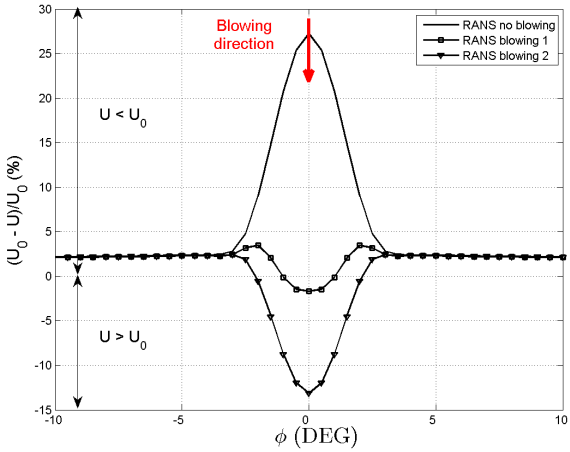

Figure 15: Velocity deficit of the pylon wake at mid-span with blowing

As pointed out in figures 16a and 16b, depending on the blown mass flow, the unsteady-loading noise is not affected in the same way. The first, lower flow rate fulfils the primary objective of blowing. The velocity deficit being reduced, the unsteady-loading noise is much less significant, with a decrease of almost 15 dB of the maximum noise level. Thereby this justifies the choice of including all steady source mechanisms in the methodology. Indeed both steady-loading noise and thickness noise become the dominant noise contributions that should be included in the model to correctly predict the interference effects. In contrast the second higher flow rate is no longer beneficial. The blown mass flow being too high, the blades cross one or several velocity gradients and still produce unsteady-loading noise. Although the unsteady noise levels are reduced compared to the configuration without blowing, the blowing flow in this case is less optimized than for the first flow rate.

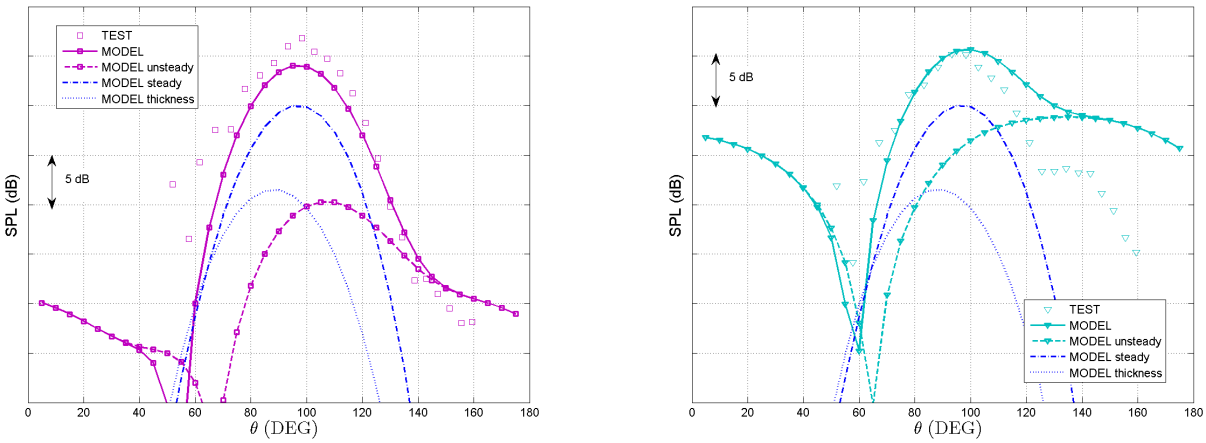

(a) 1st flow rate

(b) 2nd flow rate

Figure 16: Total noise predictions in *PylonBottom* configuration (m = 1) at $\phi = 90°$ with blowing and comparison with test data.

Considering the total noise predictions, the same conclusion can be established. Inducing a decrease of the maximum noise level of almost 5 dB, the first flow rate is more beneficial for the first BPF tone, as shown in figure 17a (grouping together the total noise predictions and the test data from figures 11a, 16a and 16b). Except downstream of the propeller, this result is not recovered in the measurements where the second flow rate is found to generate lower noise around the propeller plane than the first flow rate. This observation highlights the difficulty of the model to return the interference between all noise contributions, which is significant in this region for the first noise harmonic. This analysis is confirmed at higher BPF harmonics for which the unsteady-loading noise becomes the only significant contribution. The relative benefit of both flow rates is in this case in a good agreement with the measurements, as pointed out in figure 17b.

An optimum of the flow rate has therefore to be found. The optimization is achievable using the present analytical model but requires to keep in mind two critical points. Firstly this optimization must be performed on the total noise radiated by the front rotor including both unsteady and steady source mechanisms. To identify the most relevant blown mass flow on unsteady-loading noise only could lead to wrong conclusions. Secondly this optimization should be done for a given range of observer azimuthal angles. Indeed, as shown by previous section, the source interference affects very differently the received noise levels, depending on the azimuthal angle of the observer relative to the pylon. For a selected pylon configuration, only a range of the angular directivity could be optimized, for instance the noise radiated either to the ground or to the passengers.

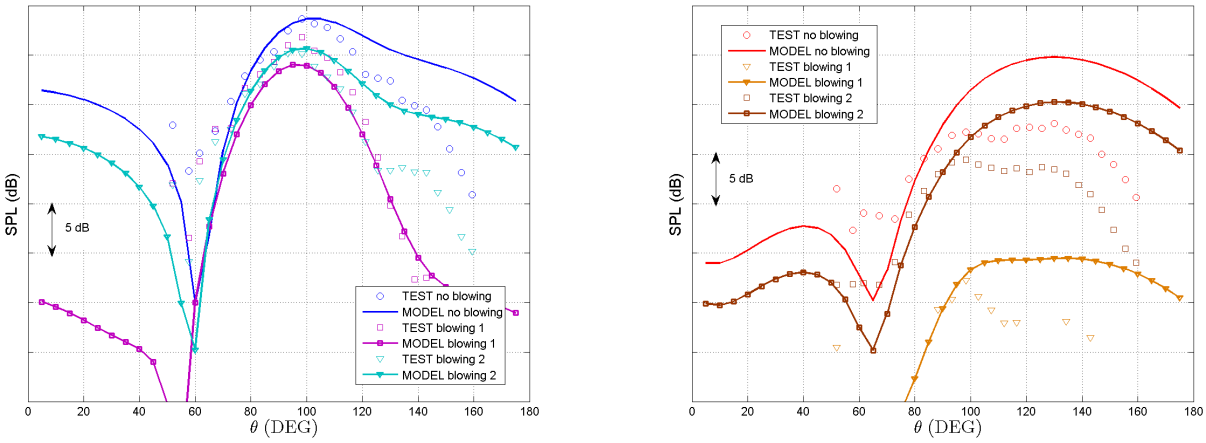

(a) m = 1 (b) m = 2

Figure 17: Blowing assessment on the total noise predictions in *PylonBottom* configuration at $\phi = 90°$ and comparison with test data.

VII. Conclusion and Future Work

The present study describes a unified, semi-analytical methodology to predict the main pylon-wake effect on the noise radiated by CROR propulsion systems, at the front-rotor BPF tones. The emphasis is put on the steady source mechanisms in the blade reference frame considered as significant at the investigated angular velocities. The results stress that both the steady-loading and thickness noise interfere with the unsteady-loading noise caused by the pylon wake. This effect is crucial for specific azimuthal angles or when assessing the blowing technology. The methodology takes part in a CROR aerodynamic installation effect prediction scheme and will be assessed against the Z08 test campaign performed in 2012 at DNW. It should be completed with other identified sources generated by the integration, such as the flow distortion induced by the fuselage or by a non-zero incidence. In priority the sensitivity to the pylon-wake parameters has to be evaluated in order to relate the noise prediction variations to changes of the velocity deficit extracted from the numerical simulations. Finally an attempt can be made to capture some acoustic installation effects deemed effective such as the sound refraction by the propeller streamline tube.

Acknowledgments

The authors acknowledge Rolls-Royce for the fruitful collaboration in the framework of the test campaign referred to in this paper.

This work was performed within the framework of the Labex CeLyA of Université de Lyon, operated by the French National Research Agency (ANR-10-LABX-0060/ ANR-11-IDEX-0007).

References

[1]Envia, E., "NASA Open Rotor Noise Research," *14th CEAS-ASC Workshop on Aeroacoustics of high-speed aircraft propellers and open-rotors*, Warsaw, Poland, 2010.

[2]Hubbard, H. H., *Aeroacoustics of flight vehicles. Theory and practice volume 1. Noise sources*, Vol. 1, NASA Reference Publication, 1991.

[3]Carazo, A., Roger, M., and Omaïs, M., "Analytical prediction of wake-interaction noise in counter-rotation open rotors," *17th AIAA/CEAS Aeroacoustics Conference*, Portland, OR, USA, 2011.

[4]Boisard, R., Delattre, G., and Falissard, F., "Assessment of aerodynamic and aero-acoustic tools for open-rotor," *14th CEAS-ASC Workshop and 5th Scientific Workshop of X3*, Warsaw, Poland, 2010.

[5]Colin, Y., Carazo, A., Caruelle, B., Node-Langlois, T., and Parry, A. B., "Computational strategy for predicting CROR noise at low-speed. Part I: review of the numerical methods," *18th AIAA/CEAS Aeroacoustics Conference*, Colorado Springs, CO, USA, 2012.

Nah, doesn't talk about analytical tools

[6]Stuermer, A. and Yin, J., "Low-Speed Aerodynamics and Aeroacoustics of CROR Propulsion Systems," *15th AIAA/CEAS Aeroacoustics Conference*, Miami, FL, USA, 2009.

[7]Colin, Y., Blanc, F., Caruelle, B., Barrois, F., and Djordjevic, N., "Computational strategy for predicting CROR noise at low-speed. Part II: investigation of the noise sources computation with the chorochronic approach," *18th AIAA/CEAS Aeroacoustics Conference*, Colorado Springs, CO, USA, 2012.

[8]Ricouard, J., Julliard, E., Omaïs, M., Regnier, V., Parry, A. B., Baralon, S., "Installation effects on contra-rotating open rotor noise," *16th AIAA/CEAS Aeroacoustics Conference*, Stockholm, Sweden, 2010.

[9]Shivashankara, B. N., Johnson, D. P., and Cuthbertson, R. D., "Installation effects on counter rotating propeller noise," *AIAA, Space Programs and Technologies Conference*, Vol. 1, 1990.

[10]Woodward, R. P. and Hughes, C. E., "Noise of a model counterrotation propeller with simulated fuselage and support pylon at takeoff/approach conditions," *12th AIAA/CEAS Aeroacoustics Conference*, San Antonio, TX, USA, 1989.

[11]Ffowcs Williams, J. E. and Hawkings, D. L., "Sound generation by turbulence and surfaces in arbitrary motion," *Philosophical Transactions of the Royal Society of London A (Mathematical and Physical Sciences)*, Vol. 264, No. 1151, 1969, pp. 321–342.

[12]Isom, M. P., "The theory of sound radiated by a hovering transonic helicopter blade." *Polytechnic Institute of New York Report Poly-AEIAM No. 75-4.*, 1975.

[13]Farassat, F., "The derivation of a thickness noise formula for the far-field by Isom," *Journal of Sound and Vibration*, Vol. 64, No. 1, 1979, pp. 159–160.

[14]Hanson, D. B. and Fink, M. R., "The importance of quadrupole sources in prediction of transonic tip speed propeller noise," *Journal of Sound and Vibration*, Vol. 62, No. 1, 1979, pp. 19–38.

[15]Hanson, D. B., "Noise of Counter-Rotation Propellers," *Journal of Aircraft*, Vol. 22, No. 7, 1985, pp. 609–617.

[16]Hanson, D. B. and Parzych, D. J., "Theory for noise of propellers in angular inflow with parametric studies and experimental verification," *Final Report United Technologies Corp., Windsor Locks, CT. Standard Div.*, Vol. 1, 1993.

[17]Ghorbaniasl, G. and Lacor, C., "A moving medium formulation for prediction of propeller noise at incidence," *Journal of Sound and Vibration*, Vol. 331, No. 1, 2012, pp. 117–137.

[18]Khelladi, S. and Bakir, F., "A Consistency Test of Thickness and Loading Noise Codes Using Ffowcs Williams and Hawkings Equation," *Advances in Acoustics and Vibration*, Vol. 2010, 2010.

[19]Ghorbaniasl, G. and Hirsch, C., "Validation of a time domain formulation for propeller noise prediction," *International Journal of Aeroacoustics*, Vol. 5, No. 4, 2006, pp. 295–310.

[20]Amiet, R. K., "High frequency thin-airfoil theory for subsonic flow," *AIAA Journal*, Vol. 14, No. 8, 1976, pp. 1076–1082.

[21]Beaumier, P., "Numerical Tools Developed at ONERA for the Aerodynamic Assessment of Propellers and Counter-Rotating Open Rotors," *28th Congress of the International Council of the Aeronautical Sciences*, Brisbane, Australia, 2012.

[22]Hanson, D. B., "Propeller noise caused by blade tip radial forces," *10th AIAA/CEAS Aeroacoustics Conference*, Seattle, WA, USA, 1986.

[23]Drela, M., "XFOIL: An analysis and design system for low Reynolds number airfoils," *Low Reynolds number aerodynamics*, Springer, 1989, pp. 1–12.

[24]Prieur, J. and Rahier, G., "Aeroacoustic integral methods, formulation and efficient numerical implementation," *Aerospace Science and Technology*, Vol. 5, No. 7, 2001, pp. 457–468.

[25]Jaouani, N., Roger, M., Nodé-Langlois, T., and Serre, G., "Analytical prediction of pylon-wake effect in counter-rotating open rotor tonal noise," *12ème Congrès Français d'Acoustique*, Poitiers, France, 2014.